RSC Advances

PAPER

View Article Online
View Journal | View Issue

Cite this: *RSC Adv.*, 2014, **4**, 37547

Specific and photostable rhodamine-based tracker for 3D video imaging of single acidic organelles†

Zhiwei Ye, Yi Xiao,* Haiying Guo and Chao Wang

Received 4th May 2014
Accepted 31st July 2014

DOI: 10.1039/c4ra04091k

www.rsc.org/advances

Three-dimensional video imaging has emerged as an indispensable tool for real-time monitoring of dynamic acidic organelles. However, the limitation of video imaging is the absence of a specific stain for acidic organelle trackers. The aim of this work was to investigate the applicability of a potential acidic organelle tracker, **Lyso-R**, in three-dimensional video imaging in live cells. In a close examination of three differently designed rhodamine dyes, **Lyso-R** outperformed the other two with a suitable pK_a value and higher membrane permeability. The uninterrupted fluorescence of **Lyso-R** towards macromolecules, *e.g.* lecithin and proteins, led to higher specificity and signal-to-background ratio than LysoTracker DND 189 and DND 99 for imaging acidic organelles. In addition, **Lyso-R** was photostable, and MTT assays confirmed its low toxicity towards cells. Inspired by these facts, three-dimensional tracking of a single acidic organelle in a live cell was obtained by staining with **Lyso-R** under confocal microscopy. The measurement of this organelle demonstrated that the distance change of the organelle centroid on *XY* plane was sharper than its depth change. The usage of **Lyso-R** was further extended with two-dimensional video imaging of acidic organelles during various cell metabolisms. All of these results demonstrate the potential applicability of **Lyso-R** as a three-dimensional imaging tracker of acidic organelles.

Introduction

Acidic organelles include lysosomes, late endosomes and other acidic compartments.[1,2] These organelles continuously perform complex transformations in morphology and cooperate with other organelles to serve various functions, like the repair of plasma membranes, the turnover of cellular proteins, and the down-regulation of surface receptors.[3,4] These dynamic changes are crucial for their functions and also reflect their health status.[5,6] The characteristic of these organelles is their acidic lumens, which is maintained by the proton pump from the organelle's membrane. In order to visualize the acidic organelles and their cooperation, a series of trackers[7–12] attached with a weak base group have been developed for acidic organelles. However, these trackers are commonly used in two-dimensional (2D) imaging, which leads to omission of critical details on *Z* dimension. To the best of our knowledge, their usage in three-dimensional (3D) video imaging (3D video imaging involves time-lapse imaging) of acidic organelles has rarely been reported.

The unsatisfactory property of conventional trackers for acidic organelles, namely, less specificity in staining, has restricted their real-time video imaging ability in three dimensions.[13] On the one hand, the non-specific stain of commercial trackers in cells generates the mixed signals of specific fluorescence and nonspecific background fluorescence noise, which decreases the resolution and makes 3D video imaging unreliable. The rigid polycyclic aromatic structures of LysoTrackers, like DND 99 and DND 189, generates a strong tendency of accumulating in the hydrophobic cavities of proteins or lipids, leading to their poor specificity. Moreover, DND 99 photodegrades to another emissive species during imaging,[14] which further reduces its signal-to-background ratio in imaging. Although conjugating highly hydrophilic groups to some extent addresses this problem, it results in another serious problem of membrane impermeability. On the other hand, 3D video imaging without sacrificing lateral resolution requires trackers to emit more photons before photobleaching than in 2D imaging or 3D imaging. Although 3D video imaging and 3D imaging are same in nature: a collection of photons, 3D video imaging involves a stack of 3D images at different time points; moreover, 3D video imaging requires a high-photostability tracker. Poor photostability of trackers, like Neutral Red (NR), results in fast photobleaching before emitting enough photons for 3D video imaging. Thus, this paper describes a better tracker to replace the commercial ones for 3D video imaging of single acidic organelles, as well as series of video imaging examples of acidic organelles during various cell metabolisms.

State Key Laboratory of Fine Chemicals, Dalian University of Technology, 2 Linggong Road, Dalian 116024, China. E-mail: xiaoyi@dlut.edu.cn

† Electronic supplementary information (ESI) available: The detailed characterization of compounds and additional figures for the manuscript. See DOI: 10.1039/c4ra04091k

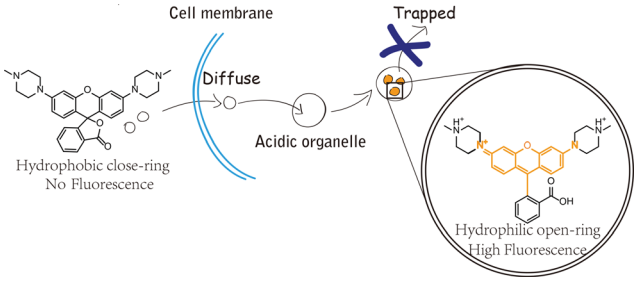

Chart 1 Working principles of **Lyso-R**, which keeps a good balance between the cell-membrane permeability and the specificity of localization in acidic organelles.

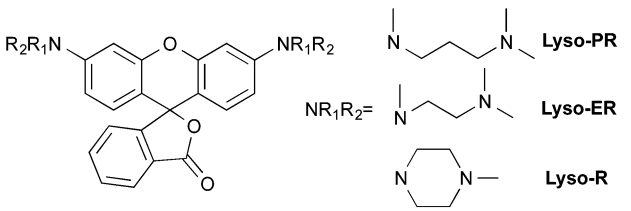

Chart 2 Structures of designing trackers, **Lyso-ER**, **Lyso-PR** and **Lyso-R**.

Results and discussion

Molecular design

The design strategy is exhibited in Chart 1 (**Lyso-R** has been published[15] before but without any further applicable tests). Firstly, the fluorophore moiety of rhodamine, a well-known laser dye, has moderate photostability and strong fluorescence. Secondly, owing to the specialty of forming hydrophobic leuco structure, the tracker freely diffuses through the plasma membrane and the organelle's membrane. Lastly, but most importantly, two conjugated alkalescent amino moieties significantly contribute to the specific stain of the acidic organelle. Outside the acidic environment, the free amino group quenches the fluorescence through PET[16,17] (photoinduced electron transfer) processes. Inside the acidic organelles, the protonation of the amino moieties converts the hydrophobic trackers into highly hydrophilic molecules emitting strong fluorescence; consequently, the hydrophilicity of trackers stabilizes their retention to prevent them from intercalating into hydrophobic domains. In fact, even if trace quantities of trackers are distributed outside those organelles, their fluorescence will be negligible due to the PET processes. In order to identify the appropriate functionality, we designed three rhodamine-based trackers, **Lyso-R**, **Lyso-ER** and **Lyso-PR**, which are shown in Chart 2.

Lyso-R surpasses the other two trackers in cellular staining

Although trackers with basic groups are potentially toxic towards cells, our designed trackers exhibits low toxicity towards cells in MTT (3-(4,5-dimethylthiazol-2-yl)-2,5-diphenyltetrazolium bromide) assays (ESI Fig. S1b†). At either a minimum concentration of 1 μM or a maximum concentration of 5 μM, up to 85% of the dye-incubated cells are alive after 24 hours (only **Lyso-PR** exhibits 70% cell survival). The low toxicity indicates the potential property of trackers for biological imaging.

Compared with **Lyso-ER** and **Lyso-PR**, **Lyso-R** exhibits far better applicability for acidic staining (ESI Fig. S1†). As shown in Table 1, **Lyso-R** is hydrophobic in neutral aqueous solution with a positive log *P* value of 0.85, while the other two trackers are slightly hydrophilic in the same aqueous solution. This hydrophobicity of **Lyso-R** drives the tracker to diffuse through the membranes *in vivo*, which is confirmed by the cell staining experiment shown in ESI Fig. S1d.† The other two trackers, hindered due to their hydrophilicity are membrane-impermeable as no fluorescence is detected in the same experiment. This result is further confirmed by their higher pK_a value (7.82 and 9.95, respectively) than **Lyso-R** (6.11). This pK_a value result suggests that **Lyso-ER** and **Lyso-PR** exist in positively charged and membrane-impermeable forms in neutral media (pH around 7), while **Lyso-R** retains its ring-closed hydrophobic form to diffuse through the membranes. Furthermore, **Lyso-R** owns high quantum yields of 0.729, as well as a high absorption cross section of 2.9×10^{-19} cm^2 at 526 nm in aqueous solution of pH 4.0. Combined with the abovementioned results, **Lyso-R** surpasses the other two trackers owing to its better cell permeability.

Lyso-R's specificity and photostability: co-localization and comparison with commercial trackers

Firstly, **Lyso-R** exhibits a good quantum yield and absorption cross-section compared with commercial trackers (NR, DND

Table 1 Photophysical properties of **Lyso-R**, **Lyso-PR** and **Lyso-ER**

Compound	log P^a	p$K_a{}^b$	Absorb peak^b (nm)	Fluorescent peak^b (nm)	Stokes shift (nm)	Quantum yields^c	Absorption cross section^b ($\times 10^{-19}$ cm^2)
Lyso-R	0.85	6.11	526	557	31	0.73	2.9
Lyso-ER	−0.38	7.82	533	555	22	0.80	1.8
Lyso-PR	−0.58	9.95	543	565	22	0.53	3.0

^{a} log *P* tests in neutral aqueous solutions; log *P* (logarithm of octanol–water partition coefficient) value indicates the hydrophobicity or hydrophilicity of compound. ^{b} All labeled data are measured at a concentration of 5 μM in aqueous solution of pH = 4.0. ^{c} Quantum yields are measured in aqueous solution of pH = 4.0 using fluorescein as a standard (Φ_{fl} = 0.92 in 0.1 M NaOH solution).[18]

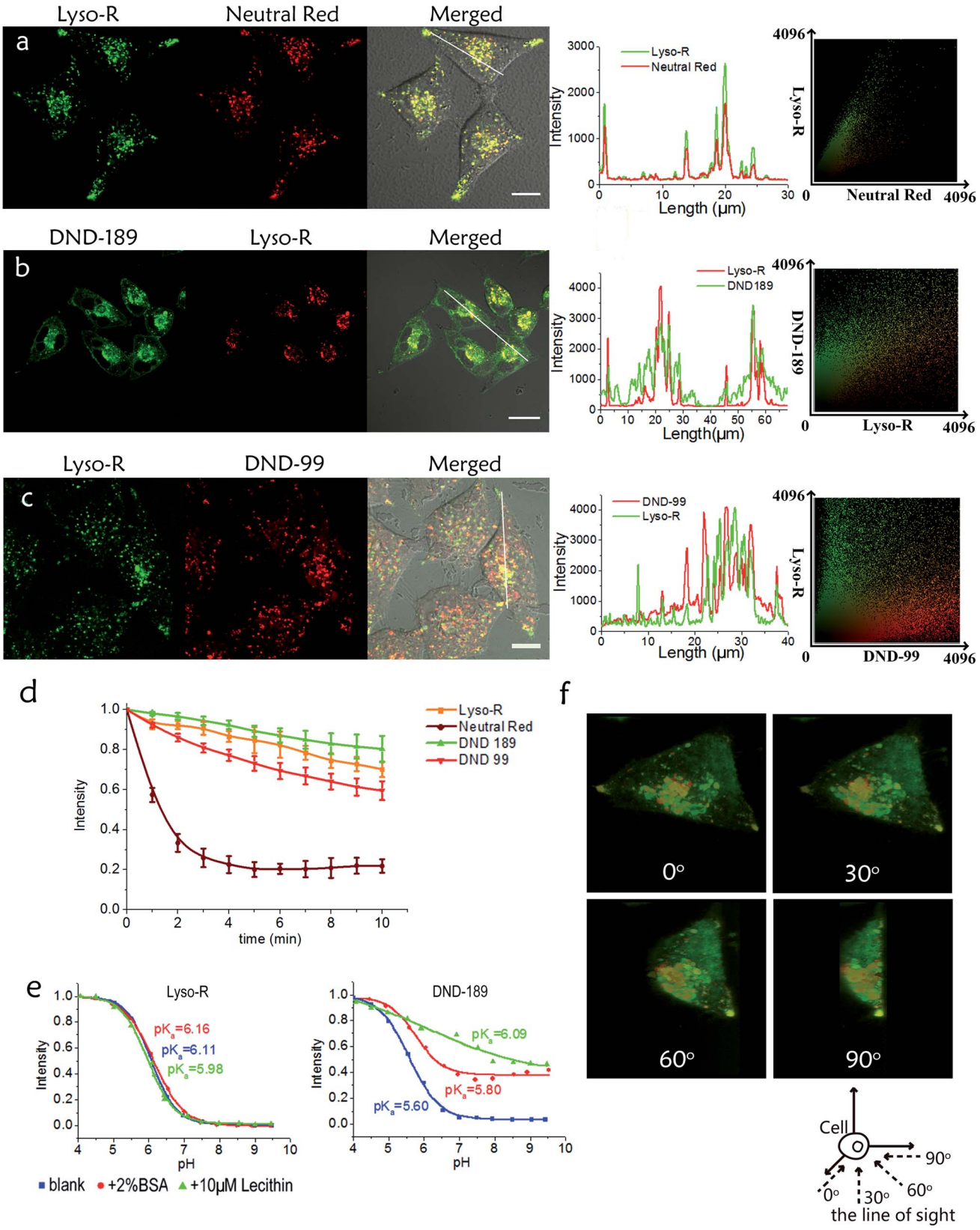

Fig. 1 Applicability of **Lyso-R** for 3D video imaging of acidic organelles. (a) Colocalization of **Lyso-R** (0.25 μM, λ_{ex} = 488 nm, λ_{em} = 530 nm–570 nm) with NR (0.25 μM, λ_{ex} = 559 nm, λ_{em} = 570–590 nm) in MCF-7 cells. Sequential images exhibit the two-channel confocal images, the merged image, intensity profile of ROIs across cells and the intensity correlation profile of **Lyso-R** and NR (the intensity correlation profile indicates the correlation between two fluorescent images. When two fluorescent images have perfect correlation, the plots perfectly overlap the diagonal line[22]). (b) Colocalization of **Lyso-R** (0.25 μM, λ_{ex} = 515 nm, λ_{em} = 530 nm–570 nm) with DND 189 (0.25 μM, λ_{ex} = 458 nm, λ_{em} = 470

Table 2 Co-localization and signal-to-background results of **Lyso-R**, DND 99, DND 189 and NR calculated from confocal images

Compound	Pearson's coefficient[a]	Manders' coefficient[a]	SBR[b]
Lyso-R	—	—	12.36 ± 1.8
Neutral red	0.89 ± 0.02	0.94 ± 0.01	—
DND 189	0.82 ± 0.04	0.87 ± 0.03	7.04 ± 1.43
DND 99	0.71 ± 0.11	0.81 ± 0.06	4.57 ± 1.07

[a] Colocalization analysis of DND 189, DND 99 or NR with **Lyso-R** in MCF-7 cells (n = 3, ±: SEM). Pearson correlation coefficient and Manders' overlap coefficient are used to quantify the co-localization of two dyes and a perfect colocalization means a value of 1 for both coefficients.[19–21] [b] SBR (signal-to-background ratio) values are calculated from the average signal divided by the background in confocal images (n = 18, ±: SEM).

189 and DND 99) listed in ESI Table S1.† Secondly, colocalization experiments confirm the specificity of **Lyso-R** towards acidic organelles. There is a close synchrony between **Lyso-R** and commercial trackers in Fig. 1a–c. This result is also supported by high Manders' coefficients in Table 2. The higher Manders' coefficients of NR and **Lyso-R** suggest an analogous stain between them. Generally, rhodamine dyes exhibit specific affinity to mitochondria, but that is not true for **Lyso-R**. In ESI Fig. S3,† **Lyso-R** exhibits a different segregated stain from tetramethyl rhodamine (TMRM), a standard mitochondrial tracker.

According to the photostability analysis in Fig. 1d, **Lyso-R** owns suitable photostability for long time imaging. In order to demonstrate the photostability of **Lyso-R**, the photostable trackers[23–25] DND 189 and DND 99, as well as the photo-unstable tracker Neutral Red, are chosen for photostability comparison. After successive ten minute imaging under continuous laser excitation, barely 30% of **Lyso-R**'s origin intensity is quenched, which is close to the photostable LysoTracker DND 99 and DND 189 and far better than Neutral Red. Thus, photostability will not restrict **Lyso-R**'s applications on 3D video imaging of acid organelles.

In Fig. 1b and f, there is a sharp contrast between the non-specific stain of DND 189 and specific stain of **Lyso-R**. In Fig. 1b, while DND 189 exhibits diffusive and continuous fluorescence signals in broad intracellular regions, the fluorescence of **Lyso-R** appears in the separated and punctual areas, consistent with the characteristics of the acidic organelles. Thus, the colocalization is not so close, supported by the relatively low Manders' coefficients (0.87 ± 0.03). Because good specificity is necessary for 3D imaging, a 3D colocalization experiment is conducted to compare the stain from DND 189 and **Lyso-R** (rotating around the Z axis in Fig. 1f and ESI movie 1†). Fluorescence signals of **Lyso-R** exhibit some globular structures, but DND 189 presents a cloud of continuous fluorescent regions with indefinite outlines.

To further understand the factors influencing the specificity in the acidic organelle's staining, a comparison study on the effects of pH, and protein and lipid concentrations on the fluorescence properties of **Lyso-R** and DND 189 is conducted. As shown in Fig. 1e, in the pH range from 7.5 to 4.5, **Lyso-R** shows a 39 times enhancement with a decrease in pH value independent of the presence or absence of BSA (representing proteins) or lecithin (representing lipids). In contrast, the plots of DND 189 exhibit high sensitivity towards the presence of BSA or lecithin. Not only the pK_a values vary considerably, but the fluorescence increase tendencies are also different. For example, in the presence of lecithin, the fluorescence intensity of DND 189 at pH of 4.5 is only 1.5 times higher than at pH of 7.5, which to some extent explains the non-negligible, non-specific stain of the dye in the cells. This pK_a plot change is possibly caused by the affinity between the hydrophobic cavities of macromolecules and the hydrophobic molecule of DND 189. The abovementioned results confirm the origin of the **Lyso-R**'s specific stain of acidic organelles: the independence of significant fluorescence enhancement from other macromolecules. Moreover, in a practical cellular environment the pH value of organelles changes with time. Trackers with a fluorescence intensity influenced by protein or lipid are unsuitable for application to pH evaluation of acidic organelles in live cells. Thus, **Lyso-R** is capable of the quantitative evaluation of the pH of acidic organelles as further confirmed in ESI Fig. S7.†

To evaluate the background strength of **Lyso-R**, we calculate the signal-to-background ratio of the three dyes (**Lyso-R**, DND 189 and DND 99) shown in Fig. 2. First, we identify those high-fluorescence regions of interest, representing the acidic organelles, and the same-size region of low fluorescence, representing the background signal. Then, these data are processed through the algorithm mentioned in the experimental section to obtain the SBR value. Among all the three dyes, **Lyso-R** exhibits the highest signal-to-background ratio (12.36 ± 1.8), which suggests that it is the most specific for staining acidic organelles. Consistent with the abovementioned pK_a value, the SBR of DND 189 is the lowest, making DND 189 potentially inapplicable for some noisy environments. DND 99 has also been found to have an unknown mechanism of photodegradation to another emissive species,[14] which possibly reduces its signal-to-background ratio. With the combination of these facts and the possible unquenched fluorescence in a physiologically neutral environment, DND 99 exhibits a moderate SBR value, between **Lyso-R** and DND 189.

nm–510 nm) in MCF-7 cells. Sequential images exhibit the two-channel confocal images, the merged image, intensity profile of ROIs across cells and the intensity correlation profile of **Lyso-R** and DND 189. (c) Co-localization of **Lyso-R** (0.25 μM, λ_{ex} = 488 nm, λ_{em} = 530–570 nm) with DND 99 (0.25 μM, λ_{ex} = 559 nm, λ_{em} = 570–630 nm) in MCF-7 cells. Sequential images exhibit the two-channel confocal images, the merged image, intensity profile of ROIs across cells and the intensity correlation profile of **Lyso-R** and DND 99. (d) Photostability comparison of four dyes, **Lyso-R**, DND 189, DND 99 and NR in live cells under continuous laser excitation (approximately 0.24 mW cm^{-2}) (n = 3, see details in the experimental section). (e) pK_a plot of **Lyso-R** and DND 189 at 1 μM in aqueous solution, 2% bovine serum albumin (BSA) and 10 μM lecithin, respectively. (f) Colocalization of **Lyso-R** (red) and DND 189 (green) in 3D image rotates from 0° to 90°, respectively. Scale bar: 10 μm (a and c), 20 μm (b).

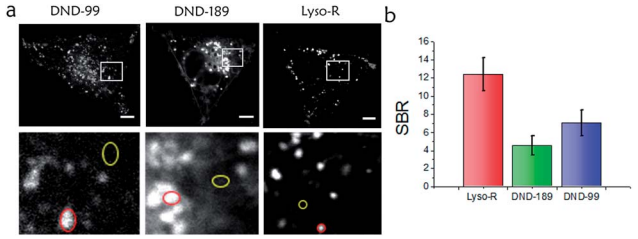

Fig. 2 Quantitative analysis of signal-to-background ratio (SBR) of **Lyso-R**, DND 189 and DND 99 for the *in vivo* acidic organelle's targeting ability. (a) Images acquired from confocal microscopy. Magnification images of the white boxes in the upper images are shown in the images below. In those below images, the average of signal and noise were calculated from the fluorescent intensities in the circle representing the acidic organelles (red circle) and the background area (yellow circle), respectively. The SBR of a single dye was obtained from the average signal divided by the background (see Experimental). (b) SBR value of **Lyso-R**, DND 189 and DND 99 for the acidic organelle's targeting ability ($n = 18$ processes). Scale bar: 5 μm.

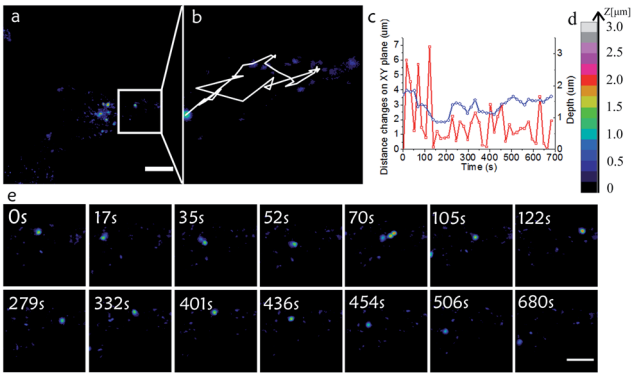

Fig. 3 3D tracking of a single acidic organelle in **Lyso-R** (0.25 μM, $\lambda_{ex} =$ 515 nm, $\lambda_{em} =$ 530–570 nm)-stained MCF-7 cells. The tracking rate is approximately 17.5 seconds per image. The resolution of the captured images is 800 × 800 pixels. (a) The MCF-7 cell's panorama. (b) Tracking trajectory of the organelle projects on the *XY* plane. (c) The *XY* distance change and depth of the organelle centroid *vs.* time. (d) The calibration bar of color to its depth, respectively. (e) Image sequence of the organelle. Scale bar: 10 μm (a), 5 μm (e).

The cytotoxicity of **Lyso-R** is further evaluated in ESI Fig. S8.† As the data in ESI Fig. S8† shows, no obvious cytotoxicity is observed for **Lyso-R**. The cell variability of MCF-7 cells is 93.4% for 24 h and 92.2% for 48 h at the concentrations of 1 μM. The concentration experiment on the cell variability of MCF-7 cells also suggests a good biocompatibility of **Lyso-R** for cell variability up to 85% at concentrations as high as 10 μM. Combined with the abovementioned results, **Lyso-R** exhibits good biocompatibility, significant specificity towards acidic organelles and suitable photostability for 3D video imaging. In order to further confirm this potential for video imaging of acidic organelles, the application of **Lyso-R** for real-time video imaging of various biological situations is analyzed and discussed.

3D tracking of single acidic organelles in MCF-7 cells by using Lyso-R

By using **Lyso-R**, a 3D video tracking of single acidic organelles of MCF-7 cells under confocal microscopy is achieved, as exhibited in Fig. 3 (and also in ESI movie 2 and 2a†). To prepare a 3D track of a single acidic organelle, we carefully choose an organelle with both the highest signal (brighter than surrounding organelles) and the largest size (nearly 1 μm). Moreover, in the surrounding area, there are no other acidic organelles with higher signals and larger size. Thus, despite the long interval between each image, the tracked organelle in each image would be the same organelle. The sequential images, shown in Fig. 3e, present the average depth of the organelle during sequential time intervals. When these images are combined with a time resolution of 17.44 s, the 3D confocal video is generated in ESI movie 2 and 2a.†

In order to evaluate the depth of a single acidic organelle, we propose a concise algorithm shown in the experimental section. Through this algorithm, the depth of the organelle centroid over time is recorded in Fig. 3c along with the *XY* distance of the organelle centroid during the imaging time. The plot shows that the *XY* distance of this single organelle centroid changes sharper than its depth. In ESI Fig. S9,† six more acidic organelles are analyzed. All data exhibit the sharper change of the *XY* position than that of the depth. There may be two factors contributing to this. Firstly, due to the horizontal extension of the adherent cells, the length (around 30–40 μm) and width (around 15–30 μm) of the cell is longer than its depth (around 5–10 μm). The second factor may be the shape of the cytoskeleton.[26,27] Furthermore, the recorded trajectory is similar to a cycle in Fig. 3b. Above all, the successful application of **Lyso-R** in 3D track of single acidic organelles in live cells under confocal microscopy confirms the suitable photostability and strong specificity for the imaging of acidic organelles.

Lyso-R tracking by stimulation-induced tubular organelles in macrophages RAW264.7 cells

Most acidic organelles are known to be small globular structures. However, upon LPS stimulation or under starvation condition, partial globular acidic organelles, particularly lysosomes, transform into tubular shapes in microphages.[28] These

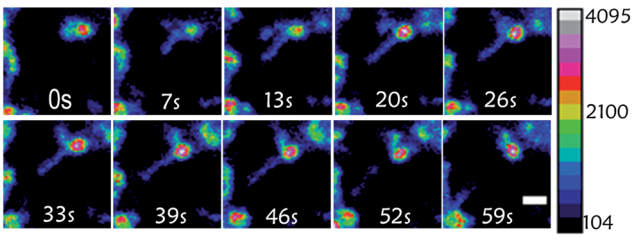

Fig. 4 Image sequences of tubular organelle formation from **Lyso-R** stained macrophages after exposing to 10 μg mL^{-1} of LPS for 1 h. These macrophages are incubated with **Lyso-R** (1.0 μm) for five minutes. Then, the dyes in the medium are washed out by PBS solutions, and next, the cells are exposed to 10 μg mL^{-1} of LPS for 1 h. The cells are imaged under continuous laser excitation for around 1 min. Scale bar: 1 μm. Color bar indicates the range from low- (black) to high-fluorescence intensity (white).

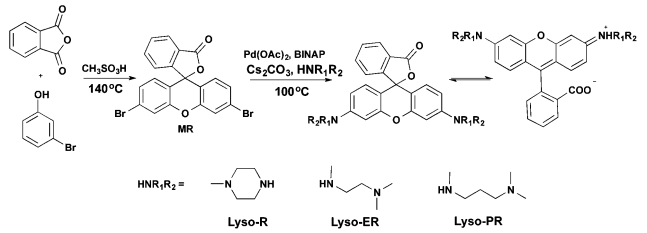

Scheme 1 Synthesis route of Lyso-R, Lyso-ER and Lyso-PR.

tubular organelles, which comprise a more motile population than normal organelles,[29] are related to metabolite transport[30] and autophagy[31] in cell metabolism.

To clearly understand this tube phenomenon, we study the tubular acidic organelles in macrophages stained with **Lyso-R** (Fig. 4, ESI Fig. S5 and ESI movie 3a and b†). In this experiment, the "bud" formation of a single tubular organelle is captured unambiguously. Different tubular organelles are stained with **Lyso-R** in ESI Fig. S5.† They exhibit low fluorescent signals compared to globular acidic organelles, suggesting their potentially higher pH value. The formation process of a single tubular organelle is fully presented in Fig. 4. Single tubular acidic organelle arises from the globular acidic organelle in less than 50 seconds, which is consistent with the former findings.[29] After maturation, it splits from the original organelle. Thus, the imaging of tubular organelles extends the application of **Lyso-R** in the video imaging of different types of acidic organelles.

Other applications of Lyso-R

To extend the applicability of **Lyso-R**, two other different acidic organelles, involving cellular dynamic processes, have been real-time imaged and some interesting and/or previously unavailable phenomena are observed. Firstly, we study the acidic organelle's behavior during lipid hydrolysis in MCF-7 cells (ESI Fig. S6 and ESI movie 4, 4a and 4b†). The concave shape of acidic organelles close to lipid droplets indicates the potential microautophagy regulation during lipid hydrolase. In addition, the two-channel video imaging suggests the multi-color video imaging ability of **Lyso-R**. Lastly, the process of the clinical medicine chloroquine, inducing pH elevation of the single acidic organelles of MCF-7 cells, is visualized for the first time in ESI Fig. S7 and ESI movie 5.† The result suggests three potential stages for incubational pharmacology of chloroquine in the MCF-7 cell. Through this video imaging, **Lyso-R** also exhibits potential applicability for pH evaluation of single acidic organelles in live cells.

Conclusions

In summary, we design a specific and photostable tracker for the 3D video imaging of acidic organelles in live cells. Firstly, three potential trackers based on rhodamine are designed and tested. After careful comparison of their pK_a value, log P value, cell permeability and cell toxicity, **Lyso-R** surpasses the other two dyes with suitable pK_a value and cell permeability. **Lyso-R** exhibits a good quantum yield and absorption cross-section compared with commercial trackers (DND 99, DND 189 and Neutral Red). **Lyso-R** also exhibits no obvious cytotoxicity in MTT experiments. The specificity of acidic organelle staining from **Lyso-R** is supported by the coefficients study in colocalization experiments between conventional trackers and **Lyso-R**. Moreover, **Lyso-R** also owns a good photostability close to conventional DND 99 and DND 189. Furthermore, in pK_a plot studies, the fluorescence of **Lyso-R** exhibits a strong independence from the presence of lecithin and proteins, while the fluorescence of DND 189 is strongly affected by them. In addition, the signal-to-background ratio of **Lyso-R** is higher than that in conventional trackers, DND 189 and DND 99. These results indicate that **Lyso-R** surpasses the conventional trackers for its specificity and photostability.

Furthermore, the 3D video imaging of a single acidic organelle in a MCF-7 cell under confocal microscopy is achieved by using **Lyso-R**. The result suggests that the movement of the organelle is sharper in the plane of focus than in the depth, and both the photostability and the specificity of **Lyso-R** are suitable for the 3D video imaging of acidic organelles. The visualization of tube phenomenon in **Lyso-R**-stained macrophages indicates a higher pH value of the tubular organelle than the original globular acidic organelle. This video imaging extends the potential applicability of **Lyso-R** for the *in vivo* imaging of acidic organelles under confocal microscopy. Therefore, it is anticipated that **Lyso-R** would be useful in future acidic organelle-related research.

Currently, considerable effort is directed toward developing various molecular probes for 'static' 2D imaging of acidic organelles, including probes for two-photon imaging,[7,32–34] for the sensing of zinc ions,[35] hydrogen peroxide,[36] hydrogen sulfide,[11] nitro oxides,[10] iron pool,[37] and pH,[8,38–40] as well as for the quantification of the organelle's viscosity.[9] As demonstrated in beginning, these 2D images lose dynamic details in depth, which could be potentially significant for the understanding of acidic organelles. In this case, **Lyso-R** is a reliable tracker for the 3D co-tracking agent of acidic organelles.

Experimental

General information

All chemicals were obtained from commercial suppliers and used without further purification. Melting points were obtained with a capillary melting-point apparatus in open-ended capillaries and are uncorrected. ^{1}H-NMR and ^{13}C-NMR were measured in CD_3OD with TMS as an internal reference. Multiplicities of signals are described in the following manner: s – singlet, br. s – broad singlet, d – doublet, t – triplet, and m – multiplet. Coupling constants (J) are given in Hz. Column chromatography was performed with silica gel (200–300 mesh).

Quantum yields

Fluorescence quantum yields were determined using fluorescein (in 0.1 M NaOH, $\Phi = 0.92$) as a reference.[18] The given

quantum yields were calculated using the following equation[41,42] with the absorption maximum 0.02–0.05.

$$\Phi_{fl}^{sample} = \Phi_{fl}^{standard} Abs^{standard} \Sigma[F^{sample}] / Abs^{sample} \Sigma[F^{standard}] \quad (1)$$

Φ_{fl} stands for the quantum yields of the tracker (sample) and the fluorescein (standard). Abs stands for the absorption value recorded at the excited wavelength. F denotes fluorescence intensity at each wavelength, and $\Sigma[F]$ was calculated by the summation of fluorescence intensity.[42]

Synthesis

The synthesis route is shown in Scheme 1.

MR. MR was synthesized according to the literature[43] (compound 8 in literature).

*General procedure for **Lyso-R**, **Lyso-ER** and **Lyso-PR**.* The procedure for **Lyso-R** is representative. To a 50 mL Schlenk flask, MR (300 mg, 0.65 mmol, 1 eq.), $Pd(OAc)_2$ (29 mg, 0.13 mmol, 0.2 eq.), BINAP (125 mg, 0.20 mmol, 0.3 eq.), and Cs_2CO_3 (847 mg, 2.6 mmol, 4.0 eq.) were added. Then, the flask was evacuated with nitrogen (3×). Toluene (20 mL) and *N*-methyl piperazine (0.5 mL, 3.81 mmol, 5.9 eq.) were added, and the reaction was stirred at 110 °C for 24 h. It was cooled to room temperature and washed thrice with saturated Na_2CO_3 solution. Then, the organic layer was dried over $MgSO_4$. The solvent was evaporated, and the residue was purified using silica gel column chromatography with eluent CH_2Cl_2–CH_3OH–triethylamine (v/v/v = 40 : 1 : 1) to afford **Lyso-R** (136 mg, 42%). mp 97–99 °C. ^{1}H NMR (400 MHz, CD_3OD) δ 8.01 (d, J = 7.3 Hz, 1H), 7.79–7.61 (m, 2H), 7.17 (d, J = 6.9 Hz, 1H), 6.76 (d, J = 1.6 Hz, 2H), 6.74–6.59 (m, 4H), 3.31 (s, 8H), 2.58 (s, 8H), 2.34 (s, 6H). ^{13}C NMR (100 MHz, CD_3OD) δ 171.0, 153.8, 135.5, 130.6, 129.6, 126.0, 125.2, 113.0, 110.7, 102.6, 96.9, 55.2, 48.2, 45.9. TOF-MS-ES(+) calcd for $C_{30}H_{33}N_4O_3$ 497.2553 found 497.2549.

Lyso-ER (85 mg, 26%). mp 86–89 °C. ^{1}H NMR (400 MHz, CD_3OD) δ 8.01 (d, J = 7.3 Hz, 1H), 7.79–7.61 (m, 2H), 7.17 (d, J = 6.9 Hz, 1H), 6.76 (d, J = 1.6 Hz, 2H), 6.74–6.59 (m, 4H), 3.31 (s, 8H), 2.58 (s, 8H), 2.34 (s, 6H). ^{13}C NMR (100 MHz, CD_3OD) δ 161.2, 159.8, 135.3, 135.1, 134.9, 133.9, 133.5, 132.8, 132.6, 117.3, 117.2, 101.0, 57.7, 50.5, 47.4, 42.3. TOF-MS-ES(+) calcd for $C_{30}H_{37}N_4O_3$ 501.2866 found 501.2906.

Lyso-PR (108.00 mg, 31%). mp 118–120 °C. ^{1}H NMR (400 MHz, CD_3OD) δ 8.17 (d, J = 7.3 Hz, 1H), 7.69 (dt, J = 19.0, 7.3 Hz, 2H), 7.24 (dd, J = 14.5, 8.4 Hz, 3H), 7.00 (d, J = 9.4 Hz, 2H), 6.89 (s, 2H), 3.60 (dd, J = 15.8, 7.6 Hz, 4H), 3.20 (s, 6H), 3.11–3.03 (m, 4H), 2.77 (s, 12H), 2.06–1.91 (m, 4H). ^{13}C NMR (100 MHz, CD_3OD) δ 161.5, 160.1, 135.6, 134.3, 133.9, 133.6, 133.0, 117.4, 100.7, 100.0, 58.8, 53.6, 46.5, 42.2, 26.4. TOF-MS-ES(+) calcd for $C_{32}H_{41}N_4O_3$ 529.3179 found 529.3173.

Culture of cells

MCF-7 (human breast carcinoma) and RAW 264.7 (macrophages cells) were obtained from the Institute of Basic Medical Sciences (IBMS) of the Chinese Academy of Medical Sciences (CAMS) and cultured in RPMI 1640 supplemented with 10% FBS (fetal bovine serum) in an atmosphere of 5% CO_2 and 95% air at 37 °C.

Effects on cell growth/viability (MTT assay)

MCF-7 cells were cultured in RPMI 1640 medium supplemented with 10% fetal bovine serum (FBS) at 37 °C in a 5% CO_2/95% air incubator. The cells in the exponential phase of growth were seeded on 96-well cell culture plates (1.5×10^3 cells per well, 100 μL), and maintained for 12 h. Then the probe (1 μM or 5 μM, dispersed in 100 μL medium) was added to the wells and incubated for 24 h. MTT (5.0 mg mL^{-1}, 20 μL), a water-soluble tetrazolium salt, which can be transformed into colored, water-insoluble formazan crystals by mitochondrial dehydrogenases in living cells, was then added. Furthermore, after being cultured for more than 4 h, the medium was removed and 200 μL DMSO was added to dissolve the formazan crystals. The optical density (OD) was recorded by an AC100-120 Automated Microplate Reader (TECAN, Switzerland) at 570 nm (630 nm was used as the reference wavelength).

Fluorescent microscopy

MCF-7 cells or macrophages on 35 mm glass-bottom culture dishes (Φ 20 mm) were grown for 1–2 days to reach 70–90% confluency. These cells were further used in the staining comparison of the four trackers. The cells were washed thrice with PBS (phosphate buffered solution, 8.0 g L^{-1} NaCl, 0.20 g L^{-1} KCl, 0.27 g L^{-1} KH_2PO_4, 1.78 g L^{-1} $Na_2HPO_4 \cdot 2H_2O$, 1.44 g L^{-1} NaH_2PO_4, pH 7.4), and then incubated with 0.25 μM solution of fluorescent dyes in an atmosphere of 5% CO_2 and 95% air for 5 min at 37 °C. Then, the cells were washed thrice with PBS. Images were obtained with a confocal microscope with a 100× objective (NA, 1.40), C.A. 0.105–0.120 μm (pinhole size, automatically adjusted by the software) and continuous laser of 2.4 mW, subjected to deconvolution with the manufacturer's software and prepared using Adobe Photoshop 6.0 software (Adobe Systems Inc.). The detectors were four integrated confocal PMT detectors. The filters were 405/488 for 405 nm or 488 nm excitation, 405/488/559 for 559 nm excitation, and 458/515 for 515 nm excitation. Quantification was performed in individual frames after deconvolution and thresholding using ImageJ software[21] (NIH). The details of the imaging were shown in the following manner: the averaging pixel dwell time was 2 μs per pixel; PMT voltage was around 550 to 700; the size of the image was 800 × 800 pixels with a depth of 12 bit per pixel; and the scanning rate was 2.18 seconds per frame. The imaging conditions for each tracker: **Lyso-R** (λ_{ex} = 515 nm, λ_{em} = 530–570 nm), Neutral Red (λ_{ex} = 559 nm, λ_{em} = 570–590 nm), DND 189 (λ_{ex} = 458 nm, λ_{em} = 470–510 nm), DND 99 (λ_{ex} = 559 nm, λ_{em} = 570–630 nm) and TMRM (λ_{ex} = 559 nm, λ_{em} = 570–600 nm). The fluorescent image threshold of 3D tracking is 0 to 1500, while for others are 0 to 4095.

Photostability

The cells were incubated with 0.25 μM **Lyso-R**, DND 189, DND 99 or 10 μM NR (because of the low quantum yields of NR) in an atmosphere of 5% CO_2 and 95% air for 5 min at 37 °C,

respectively. The cells were washed with PBS three times to eliminate the non-stain dyes. Then, these cells were exposed to continuous laser excitation of 0.24 mW cm^{-2} for approximately 10 min. The fluorescence of the cells was recorded with an interval time of 1 min. The photostability experiment for each dye was conducted three times.

SBR

SBR value is calculated according to the scientific report.[44] The algorithm is as follows:

$$\mathrm{SBR} = \left(\sum_{i \in \text{signal}} I_{\mathrm{S}}^{i} \Big/ N_{\mathrm{S}} \right) \Big/ \left(\sum_{i \in \text{background}} I_{\mathrm{b}}^{i} \Big/ N_{\mathrm{b}} \right) \qquad (2)$$

N and I stand for the number of the pixels in the region of "signal" or "background" and the intensity of the pixels, respectively. S represents "signal" and b represents "background" or "noise." All acquired images were taken in the same method as illustrated in the fluorescent imaging. In such images, the strongest signals were taken as the "signal" region in the red circle as in Fig. 2a, while the relative low fluorescence regions inside the cell were taken as the "background" region in yellow circle. Using this method, SBR value of three trackers, **Lyso-R**, DND 189 and DND 99, were determined with a total number of 18 ($n = 18$, six spots in one image).

Tracking method for a single acidic organelle

The track was performed with the same confocal microscope (0.3%, 2.4 mW continuous laser excitation) using the same cells in PBS and maintained at room temperature. A single frame contains eight depth images of 800 × 800 pixels, which individually needs 2.181 s of photo time. Thus, a frame of the video was captured every 17.45 s. A single frame was generated from these images by using "Max Intensity" Z projection in ImageJ.[45] These frames were thresholded by ImageJ so that the depth on individual frames is depicted on a colour scale. Colours run from hot (white) at high depth through to cold (blue) at low depth. They were further converted to AVI videos (ESI movie 2 and 2a†) using ImageJ at 8 frame per second using JPEG compression.

As the depth of an acidic organelle is judged by its fluorescent intensity in different depth images, a weight average method is used to calculate the average depth of a single organelle during the imaging time obtained from series depth images.

$$\mathrm{Depth}(\mu\mathrm{m}) = \sum_{i=1}^{7} \frac{I_i}{\sum_{n=1}^{7} I_n} \times D_i \qquad (3)$$

I_i and I_n stand for the mean fluorescent intensity of a single acidic organelle from different depth images. D_i stands for the depth value of various depth images.

The depth curves in Fig. 3c were calculated using this algorithm.

Real-time microscopy

The real-time video imaging was conducted with the same microscope and the same method for the aforementioned cell growth. The frame of the video was captured every 2.18 seconds with the same aforementioned illustrated imaging conditions except for the 3D tracking case, which has been separately described. The video frame rate for ESI movie 2, 2a, 3a, 3b, 4, 4a and 4b† were 8 frame per second. The video frame rate of ESI movie 5† was 80 frame per second. Then, all movies were further merged and compressed to AVI files by ImageJ.

Abbreviations

TLC	thin layer chromatography
TMRM	tetramethylrhodamine
SBR	signal to background ratio
NR	Neutral Red
BINAP	(±)-2,2′-Bis(diphenylphosphino)-1,1′-binaphthalene
SEM	standard error of the mean
MTT	3-(4,5-dimethylthiazol-2-yl)-2,5-diphenyltetrazolium bromide

Acknowledgements

This work is supported by the National Natural Science Foundation of China (no. 21174022), the National Basic Research Program of China (no. 2013CB733702) and the Specialized Research Fund for the Doctoral Program of Higher Education (no. 20110041110009). We also thank Dr Liji Jin at Dalian University of Technology for his help in cell culture.

Notes and references

1 R. G. Anderson, J. R. Falck, J. L. Goldstein and M. S. Brown, *Proc. Natl. Acad. Sci. U. S. A.*, 1984, **81**, 4838–4842.
2 R. G. Anderson and L. Orci, *J. Cell Biol.*, 1988, **106**, 539–543.
3 C. Mullins and J. S. Bonifacino, *BioEssays*, 2001, **23**, 333–343.
4 E.-L. Eskelinen, Y. Tanaka and P. Saftig, *Trends Cell Biol.*, 2003, **13**, 137–145.
5 U. Repnik and B. Turk, *Mitochondrion*, 2010, **10**, 662–669.
6 P. Boya, *Antioxid. Redox Signaling*, 2012, **17**, 766–774.
7 W. Yang, P. S. Chan, M. S. Chan, K. F. Li, P. K. Lo, N. K. Mak, K. W. Cheah and M. S. Wong, *Chem. Commun.*, 2013, **49**, 3428–3430.
8 L. Chen, J. Li, Z. Liu, Z. Ma, W. Zhang, L. Du, W. Xu, H. Fang and M. Li, *RSC Adv.*, 2013, **3**, 13412–13416.
9 L. Wang, Y. Xiao, W. Tian and L. Deng, *J. Am. Chem. Soc.*, 2013, **135**, 2903–2906.
10 H. Yu, Y. Xiao and L. Jin, *J. Am. Chem. Soc.*, 2012, **134**, 17486–17489.
11 T. Liu, Z. Xu, D. R. Spring and J. Cui, *Org. Lett.*, 2013, **15**, 2310–2313.
12 Z. Li, S. Wu, J. Han and S. Han, *Analyst*, 2011, **136**, 3698–3706.

13 E. T. W. Bampton, C. G. Goemans, D. Niranjan, N. Mizushima and A. M. Tolkovsky, *Autophagy*, 2005, **1**, 23–36.
14 E. C. Freundt, M. Czapiga and M. J. Lenardo, *Cell Res.*, 2007, **17**, 956–958.
15 J. B. Grimm and L. D. Lavis, *Org. Lett.*, 2011, **13**, 6354–6357.
16 A. Loudet and K. Burgess, *Chem. Rev.*, 2007, **107**, 4891–4932.
17 Y. Koide, Y. Urano, K. Hanaoka, T. Terai and T. Nagano, *ACS Chem. Biol.*, 2011, **6**, 600–608.
18 D. Magde, R. Wong and P. G. Seybold, *Photochem. Photobiol.*, 2002, **75**, 327–334.
19 E. Manders, F. Verbeek and J. Aten, *J. Microsc.*, 1993, **169**, 375–382.
20 J. Adler and I. Parmryd, *Cytometry, Part A*, 2010, **77A**, 733–742.
21 A. P. French, S. Mills, R. Swarup, M. J. Bennett and T. P. Pridmore, *Nat. Protoc.*, 2008, **3**, 619–628.
22 Q. Li, A. Lau, T. J. Morris, L. Guo, C. B. Fordyce and E. F. Stanley, *J. Neurosci.*, 2004, **24**, 4070–4081.
23 T. Yogo, Y. Urano, Y. Ishitsuka, F. Maniwa and T. Nagano, *J. Am. Chem. Soc.*, 2005, **127**, 12162–12163.
24 I. García-Moreno, F. Amat-Guerri, M. Liras, A. Costela, L. Infantes, R. Sastre, F. López Arbeloa, J. Bañuelos Prieto and Í. López Arbeloa, *Adv. Funct. Mater.*, 2007, **17**, 3088–3098.
25 G. Ulrich, R. Ziessel and A. Harriman, *Angew. Chem., Int. Ed.*, 2008, **47**, 1184–1201.
26 K. Pogoda, J. Jaczewska, J. Wiltowska-Zuber, O. Klymenko, K. Zuber, M. Fornal and M. Lekka, *Eur. Biophys. J.*, 2012, **41**, 79–87.
27 T. D. Pollard, *Nature*, 2001, **409**, 842–843.
28 J. Swanson, A. Bushnell and S. C. Silverstein, *Proc. Natl. Acad. Sci. U. S. A.*, 1987, **84**, 1921–1925.
29 A. Mrakovic, J. G. Kay, W. Furuya, J. H. Brumell and R. J. Botelho, *Traffic*, 2012, **13**, 1667–1679.
30 X. Li, A. G. Garrity and H. Xu, *J. Physiol.*, 2013, **591**, 4389–4401.
31 L. Yu, C. K. McPhee, L. Zheng, G. A. Mardones, Y. Rong, J. Peng, N. Mi, Y. Zhao, Z. Liu, F. Wan, D. W. Hailey, V. Oorschot, J. Klumperman, E. H. Baehrecke and M. J. Lenardo, *Nature*, 2010, **465**, 942–946.
32 J. H. Han, S. K. Park, C. S. Lim, M. K. Park, H. J. Kim, H. M. Kim and B. R. Cho, *Chem.–Eur. J.*, 2012, **18**, 15246–15249.
33 X. Wang, D. M. Nguyen, C. O. Yanez, L. Rodriguez, H.-Y. Ahn, M. V. Bondar and K. D. Belfield, *J. Am. Chem. Soc.*, 2010, **132**, 12237–12239.
34 J. H. Son, C. S. Lim, J. H. Han, I. A. Danish, H. M. Kim and B. R. Cho, *J. Org. Chem.*, 2011, **76**, 8113–8116.
35 L. Xue, G. Li, D. Zhu, Q. Liu and H. Jiang, *Inorg. Chem.*, 2012, **51**, 10842–10849.
36 D. Song, J. M. Lim, S. Cho, S. J. Park, J. Cho, D. Kang, S. G. Rhee, Y. You and W. Nam, *Chem. Commun.*, 2012, **48**, 5449–5451.
37 S. Fakih, M. Podinovskaia, X. Kong, H. L. Collins, U. E. Schaible and R. C. Hider, *J. Med. Chem.*, 2008, **51**, 4539–4552.
38 Y. Urano, D. Asanuma, Y. Hama, Y. Koyama, T. Barrett, M. Kamiya, T. Nagano, T. Watanabe, A. Hasegawa, P. L. Choyke and H. Kobayashi, *Nat. Med.*, 2009, **15**, 104–109.
39 D. G. Smith, B. K. McMahon, R. Pal and D. Parker, *Chem. Commun.*, 2012, **48**, 8520–8522.
40 H. Zhu, J. Fan, Q. Xu, H. Li, J. Wang, P. Gao and X. Peng, *Chem. Commun.*, 2012, **48**, 11766–11768.
41 J. N. Demas and G. A. Crosby, *J. Phys. Chem.*, 1971, **75**, 991–1024.
42 T. Matsumoto, Y. Urano, T. Shoda, H. Kojima and T. Nagano, *Org. Lett.*, 2007, **9**, 3375–3377.
43 C. C. Woodroofe, M. H. Lim, W. Bu and S. J. Lippard, *Tetrahedron*, 2005, **61**, 3097–3105.
44 R. Kawakami, K. Sawada, A. Sato, T. Hibi, Y. Kozawa, S. Sato, H. Yokoyama and T. Nemoto, *Sci. Rep.*, 2013, **3**, 1014.
45 C. A. Schneider, W. S. Rasband and K. W. Eliceiri, *Nat. Methods*, 2012, **9**, 671–675.